


Article

Silver Binding to Bacterial Glutaredoxins Observed by NMR

Stephanie M. Bilinovich¹, Daniel L. Morris^{2,†}, Jeremy W. Prokop³, Joel A. Caporoso⁴, Alexandra Taraboletti⁵, Nilubol Duangjumpa² , Matthew J. Panzner⁶, Leah P. Shriver^{7,8} and Thomas C. Leeper^{9,*}

¹ Department of Chemistry, Grand Valley State University, Allendale, MI 49401, USA; bilinovs@gvsu.edu

² Department of Chemistry and Biochemistry, The University of Akron, Akron, OH 44325, USA; daniel.morris@nih.gov (D.L.M.); nduangjumpa@gmail.com (N.D.)

³ Department of Pediatrics and Human Development, Michigan State University, Grand Rapids, MI 49503, USA; Prokopje@msu.edu

⁴ Department of Anesthesiology and Perioperative Medicine, School of Medicine, University of Pittsburgh, Pittsburgh, PA 15261, USA; jac398@pitt.edu

⁵ Division of Sciences and Mathematics, University of the District of Columbia, Washington, DC 20008, USA; alexandra.tarabolett@udc.edu

⁶ Synthomer, Akron, OH 44305, USA; matthew.panzner@synthomer.com

⁷ Departments of Chemistry, Washington University, Saint Louis, MO 63130, USA; sleah@wustl.edu

⁸ Departments of Medicine, Washington University, Saint Louis, MO 63110, USA

⁹ Department of Chemistry and Biochemistry, Kennesaw State University, Kennesaw, GA 30144, USA

* Correspondence: tleeper@kennesaw.edu; Tel.: +1-(470)-578-2258

† Current Affiliation: National Heart, Lung, and Blood Institute, NIH, Bethesda, MD 20814, USA.

Abstract: Glutaredoxins (GRXs) are a class of enzymes used in the reduction of protein thiols and the removal of reactive oxygen species. The CPYC active site of GRX is a plausible metal binding site, but was previously theorized not to bind metals due to its cis-proline configuration. We have shown that not only do several transition metals bind to the CPYC active site of the *Brucella melitensis* GRX but also report a model of a dimeric GRX in the presence of silver. This metal complex has also been characterized using enzymology, mass spectrometry, size exclusion chromatography, and molecular modeling. Metalation of GRX unwinds the end of the helix displaying the CPYC active site to accommodate dimerization in a way that is similar to iron sulfur cluster binding in related homologs and may imply that metal binding is a more common occurrence in this class of oxidoreductases than previously appreciated.

Keywords: glutaredoxin; GRX; silver ion; metal binding; NMR



Citation: Bilinovich, S.M.; Morris, D.L.; Prokop, J.W.; Caporoso, J.A.; Taraboletti, A.; Duangjumpa, N.; Panzner, M.J.; Shriver, L.P.; Leeper, T.C. Silver Binding to Bacterial Glutaredoxins Observed by NMR. *Biophysics* **2021**, *1*, 359–376. <https://doi.org/10.3390/biophysics1040027>

Academic Editor: Luciano A. Abriata

Received: 27 August 2021

Accepted: 20 September 2021

Published: 23 September 2021

Publisher's Note: MDPI stays neutral with regard to jurisdictional claims in published maps and institutional affiliations.



Copyright: © 2021 by the authors. Licensee MDPI, Basel, Switzerland. This article is an open access article distributed under the terms and conditions of the Creative Commons Attribution (CC BY) license (<https://creativecommons.org/licenses/by/4.0/>).

1. Introduction

Glutaredoxins (GRXs) are proteins that utilize dithiol reduction for maintenance of the intracellular redox state [1]. GRX's redox centers consist of either a dithiol active site (CPYC) or a monothiol active site (CGFS) with the former typically associated with oxidoreductase reactions and the latter principally associated with iron sulfur cluster formation/maturation [1–4]. GRXs have also been shown to have a role in metal detoxification [5,6] and have been implicated in several indirect and direct interactions with metals [7–9]. One such way that GRX interacts with metal ions is through the redox control of cysteines on chaperones and other metalloproteins, regulating the binding of metals such as copper [10]. ATOX1 is a copper chaperone for ATP7a and ATP7b, reliant on GRX for the reduction of thiols in the CXXC copper binding site [11]. The interaction of ATP7a and ATP7b with GRX remains dependent on the concentration of copper [12] and knockdown of GRX1 in drosophila disrupts copper homeostasis [13]. The thiols in these proteins are required for both redox maintenance and metal binding. Interestingly, most metallochaperones have similar active sites, with the general CXXC motif found throughout many proteins. This begs the question why do metal ions prefer the configuration of the CXXC motif in metallochaperones, as opposed to the CPYC site in GRX and other

thioredoxin fold proteins? One hypothesis for this specificity that had been proposed is that the proline in the GRX active site prevents metal binding and/or the dimerization required for metal transfer [14]. However, more recent research has indicated that copper ions can bind within GRX's active site unhindered by these prolines [15,16]. Instead, other metallochaperones, such as ATOX1, with a higher metal affinity, outcompete GRX for metal cations [15]. In addition, some proline-containing active site GRXs have been shown to form complexes to iron–sulfur clusters [17–20] suggesting that the notion that CPYC GRXs are always associated with redox chemistry while CGFS GRXs are always associated with metal atom/cluster transfer is an oversimplification [21]. This research suggests a potential for CPYC motifs to coordinate a variety of metal atoms, contrary to this well-defined “role” classification. This ability of CPYC sites to bind metal atoms could be a target for several metal-based drugs in use, supporting their overlapping alteration of redox systems.

One class of metal-based therapeutics, with possible antioxidant properties, employs silver ions as a treatment for infections. Silver salts have traditionally been utilized as antimicrobials, with a resurgence in modern medicine for preventing infection during the treatment of severe burn [22]. Recent research has worked towards adapting silver(I) for the treatment of drug resistant bacterial infection [23–27], and the treatment of cancers [28–31]. While the exact mechanism for silver(I) ion's effectiveness as an antimicrobial is not fully understood, multiple studies point to its ability to increase reactive oxygen species (ROS) [32–35]. Silver ions have also been shown to target small molecules containing thiol [36]. In addition, silver was implicated in the upregulation of expression of the GRX1 gene [37]. As GRXs are integral proteins in the processing of intracellular ROS and contain the CPYC site, we suggest that silver can directly target GRX proteins during this silver-mediated ROS amplification process.

2. Materials and Methods

2.1. Protein Expression and Purification

The plasmid containing the sequence for *Brucella melitensis* GRX was obtained from the Seattle Structural Genomics Center and a C70S mutation was introduced using Quick Change II site directed mutagenesis kit (Agilent, Santa Clara, CA, USA). The plasmid containing the *B. melitensis* GRX C70S mutation was transformed in to BL21(DE3) *E. coli* cells and grown in M9 minimal media supplemented with ¹⁵N ammonium chloride for chemical shift perturbation experiments or ¹⁵N ammonium chloride and ¹³C glucose for structural studies. Cells were grown at 37 °C until an OD₆₀₀ of 0.5 at which point the temperature was reduced to 18 °C, cells were induced with 1 mM isopropylthio-β-galactoside (IPTG), and grown for 18 h overnight. Cells were harvested via centrifugation, lysed via French press, and purified using a two-step His-Trap affinity purification with a buffer consisting of 20 mM Tris pH 8, 200 mM NaCl, 2 mM dithiothreitol (DTT), and 20 mM imidazole and an identical elution buffer with 400 mM imidazole. The 6x-His tag was removed using human rhinovirus (HRV 3C protease prior to a second His-Trap column to separate the tag and protein. The purified protein was exchanged into 50 mM MES buffer pH 6.5 with 2 mM DTT and concentrated to 2 mL under nitrogen gas using a stirred cell. At this point, the protein was treated with 50 mM tris(2-carboxyethyl)phosphine (TCEP) and incubated a 4 °C for 1 h then diluted to 10 mL with degassed 50 mM MES pH 6.5 and buffer exchanged in a stirred cell under nitrogen gas until the concentration of TCEP was estimated to be less than 0.01 mM. Previous samples prepared via dialysis in an argon-filled glove-bag behaved identically to those from the stirred cell so that latter method was used subsequently.

2.2. Chemical Shift Perturbation Studies

Experiments were performed on ¹⁵N labeled C70S mutant of GRX using a ¹⁵N HSQC to monitor shift changes associated with metal ions. The following metal salts and compounds were used: silver hydroxybutyrate, copper(II) chloride, copper(I) chloride, zinc(II) acetate, nickel(II) sulfate, and cobalt(II) chloride. The nickel(II), cobalt(II), and mercury(II)

chemical shift perturbation (CSP) studies were performed using 0.67 mM protein on a 500 MHz Agilent spectrometer equipped with a broadband HCN probe. The copper(I), copper(II), zinc(II), and silver(I) titration experiments were performed with 1 mM protein on a 750 MHz Agilent INOVA spectrometer equipped with a triple axis cryogenic probe. Normalized chemical shifts for the silver(I) titrated sample were calculated using the following equation: $\sqrt{\Delta\delta^2HN + 0.100 \times \Delta\delta^2N}$.

Glutathione CSP studies were performed with 1 mM ^{15}N GRX C70S premetalated to a ratio of 0.5 to 1 metal to protein. The protein was titrated with GSH up to 3.5 mM in the case of the copper metalated sample and up to 16 mM GSH for the silver metalated sample. A reference CSP of GSH with 1 mM apo protein was collected up to a concentration of 5 mM GSH. All experiments were performed on a 750 MHz Agilent Inova spectrometer equipped with a cryogenic probe.

2.3. Size Exclusion Chromatography

A 20 mL superose-12 column was calibrated with a LMW Calibration Kit (GE) in the presence of 50 mM MES pH 6.5. GRX samples were subjected to various conditions, either reduced with an excess of TCEP, 0.5 molar equivalents of silver to protein, or reduced with excess TCEP and buffer exchanged under inert gas (NMR sample preparation).

2.4. Determination of τ_c

Rotational correlation times (τ_c) were calculated from the T1 and T2 relaxation rates of the silver(I) metalated and apo protein. Experiments were measured on a 0.67 mM protein. For T1, the relaxation values were varied from 0 to 1900 ms and, for T2, the delay was varied from 10 to 110 ms. All experiments were collected on 750 MHz Agilent Inova spectrometer equipped with a cryogenic probe. Data were analyzed in CcpNMR.

2.5. Protein NMR Data Collection and Resonance Assignment

Protein assignments were performed using the standard methodology [38]. All data were collected on a 750 MHz Agilent INOVA equipped with a triple axis cryogenic probe. The following experiments were collected for sequential assignments: HNCO, HN(CA)CO, HNCA, HN(CO)CA, HNCACB, and CBCA(CO)NH. Side-chains were assigned using the HCCH-TOCSY, HBHACONH, ^{15}N , and ^{13}C NOESY-HSQC. NMR data were processed in NMRpipe [39] and analyzed via CcpNMR version 2 [40].

2.6. Structure Calculations

NOE cross peaks obtained from a ^{15}N NOESY-HSQC and ^{13}C NOESY-HSQC in 95% H_2O to D_2O mix (mix = 150 and 100 ms respectively). Dihedral angle restraints derived from $^1\text{H}\alpha$, ^{15}N , ^{13}C , and $^{13}\text{C}\beta$ assignments using DANGLE [41] were used in structure calculation, except for those residues that contained two islands in the Ramachandran plot and those in the CPYC active site. Structure calculation and automated NOE assignment were performed using CYANA [42,43]. A final ensemble of 20 structures was analyzed and deposited into the PDB [44].

2.7. Molecular Modeling of Ag Dimerized GRX

A dimer model of the PDB coordinates of the final output from CYANA were created by aligning a duplicate for each of the twenty calculated structures onto the Fe_2S_2 induced dimer of *E. coli* glutaredoxin (PDB 2WCI) using the MUSTANG algorithm [45]. This model was chosen due to the combination high-quality template (1.9 Å crystal structure) and because it had the highest sequence identity to the *B. meletensis* Grx. Initial dimer docking studies using AutoDock [46] for 50 predictions on 5 rotamer ensembles was unable to generate a single conformation with a positive binding energy; thus, the PDB dimer of 2WCI was used as an initial template. Following removal of the template structure (PDB: 2WCI), distances of the catalytic cysteines in the respective monomers of the dimer model, i.e., 16C in both, within the dimer interface were calculated; selecting the model with a

5 Å distance is optimal for Ag insertion. A Zn ion was added into the active site and a spring of 2.5 Å was added between each sulfur of 16C to the Zn. Energy minimizations were then performed on the dimer with pH of 7.4, water at 0.997 g/mL, and NaCl mass fraction of 0.9% using the AMBER03 [47] force field. Molecular dynamics (MD) simulations were then performed on the Zn (2.5 Å linked) dimer or on a single monomer of GRX for 10 nanoseconds each. The Zn was replaced with a silver atom (Van der Waals radius of 172 pm) for imaging.

2.8. Mass Spectrometry

The protein used for ESI-MS was reduced in a similar manner as those for NMR experiments, with the substitution of 50 mM ammonium acetate (pH 5.1) in place of the 50 mM MES. Samples were titrated with either zero or 0.5 equivalents of silver, at a concentration of 15 pmol/μL (15 μM). The samples were analyzed on a 5600+ TripleTOF Mass Spectrometer (AB SCIEX, Framingham, MA, USA) in positive mode. Parameters were optimized to achieve maximum sensitivity. A ToF MS scan was selected to survey scan for the mass range of 800–4000 Da, with an accumulation time of 250 ms for precursor ion acquisition. The ion source nebulizer gas (GS1) used was set at 18 psi, heater gas (GS2) was 18 psi, and the curtain gas (CUR) was 20 psi. The monomer and dimer reconstruction was processed with relative intensity via the Bio Tool Kit plugin in PeakView® (Ab Sciex).

2.9. HEDS Assay

Silver mediated inhibition of GRX activity was monitored using the bis(2-hydroxyethyl) disulfide (HEDS) assay originally proposed by Nagai and Black in 1968 [48]. The HEDS protocol followed here was adapted from Zaffagnini, et al. with the notable elimination of EDTA as a reaction component to avoid chelation of silver cations [49]. A reaction mixture containing 0.7 mM HEDS, 1 mM reduced GSH, 0.1 mg/mL BSA, 6 μg/mL GSH reductase, and 0.2 mM NADPH was assembled in 100 mM HEPES, pH 7.9. To this, silver cations were added to sample concentrations using a 50 mM silver acetate stock solution in water. The reaction mixture was separated into a sample and reference cuvette and after a 3-min incubation GRX was added to the sample cuvette with an equal amount of buffer to the reference cuvette. Activity was monitored by the GSH reductase catalyzed oxidation of NADPH at 340 nm using a Shimadzu UV-1800 spectrophotometer. Isolated GRX activity was observed from the change in absorbance at 340 nm in the sample cuvette versus the reference cuvette as a subtraction from the baseline NADPH oxidation rate in the reference cuvette. GRX activity was calculated from the first 30 s of each reaction and activity was expressed as mM of NADPH oxidized/min. Three replicates were collected for each condition and error bars were generated from the standard error.

3. Results

3.1. NMR Data Indicate That Multiple Metals Can Bind to the CPYC Active Site

The CPYC active site of GRX is similar to the CXXC metal binding motif of other metalloproteins, thus it was tested if various metals could bind to the CPYC active site. Chemical shift perturbation (CSP) studies with various transition metals (Table 1 and Supplemental Figure S1) indicate that silver(I), copper(I), copper(II), and mercury(II) ions all bound to the active site of the protein. All of the metals bind to GRX through slow exchange kinetics implying that they are relatively stable long-lived complexes. Interestingly, the CSP experiments show that many of these metals bind with stoichiometries around 0.5:1 (metal to protein). Closer analysis of titrations involving silver ions binding to GRX show major chemical shift changes occurring at the residues in the CPYC active site and adjacent to the site (Figure 1). The largest chemical shift changes occur at 13R, 18Y, and 19C, indicating that these resonances must undergo a large rearrangement to accommodate the binding of a metal ion.

Table 1. Metals tested for GRX binding.

Metal	Binds?	Binding Residues	Exchange
Ag(I)	Yes	CPYC	Slow
Cu(I)	Yes	CPYC	Slow
Cu(II)	Yes	CPYC	Slow
Hg(II)	Yes	CPYC	Slow
Co(II)	No	N/A	N/A
Ni(II)	No	N/A	N/A
Zn(II)	Possibly, precipitates	N/A	N/A

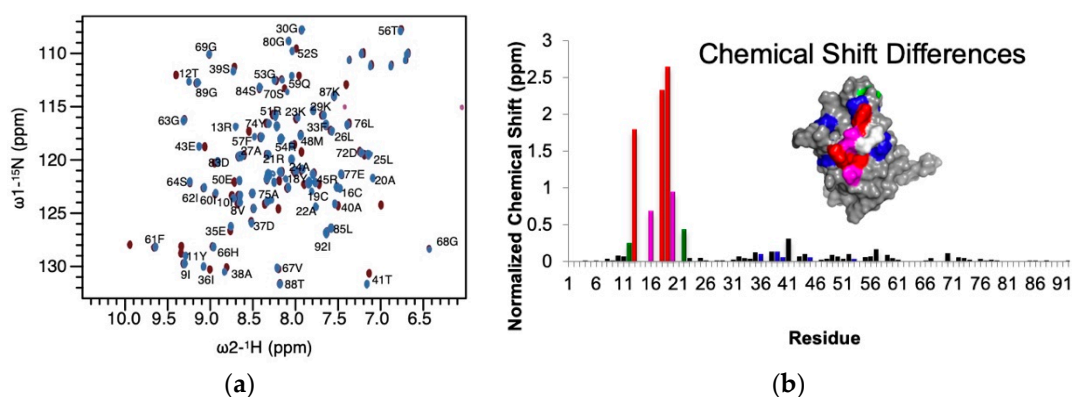


Figure 1. Chemical shift mapping of silver binding to GRX (a) HSQC of apo GRX (maroon) and 0.5 equivalents of silver (blue). (b) Normalized chemical shifts highlighted on the structure of silver metalated GRX (inset). Shifts > 1 ppm (red), 0.5 ppm (magenta), 0.25 (green), and 0.1 ppm (blue).

Both copper(I) and copper(II) had a different CSP shift pattern than that observed for silver(I), therefore, copper binding was further investigated at the CPYC active site. Copper ions are known to bind many proteins [50–57] and commonly coordinate the CXXC motif in proteins such as ATOX1 [58] and the fourth domain of the Menkes disease-associated protein [46]. Similar amino acids experienced shifts in both copper-metalated spectra, but the key residues that experienced the greatest chemical shifts were 13R, 16C, 18Y, and 19C. These, however, did not shift as extensively compared to the silver(I) titrated spectrum. The smaller shifting patterns in the copper metalated spectrums (Figure 2a) are likely a result of the smaller ionic radii of copper(I) and copper(II) in comparison to that of silver(I) (91 pm and 87 pm for Cu(I) and Cu(II) respectively and 129 pm for Ag(I)). The smaller ionic radii would require less movement of the protein to accommodate the size of the metal ion. CSP experiments for both copper(I) and copper(II) also has nearly identical spectra (Figure 2b) with only minimal line broadening in the copper (II) titrated spectrum. This is indicative of the reduction of copper(II) to copper(I) by the cysteine in GRX, although future cyclic voltammetry studies would be required to confirm this assertion. Thiols, like those found in GRX and glutathione (GSH), are effective reducing agents and GSH is known to reduce copper(II) to copper(I) [59]; what residual CSP and line broadening is present may be from residual copper(II).

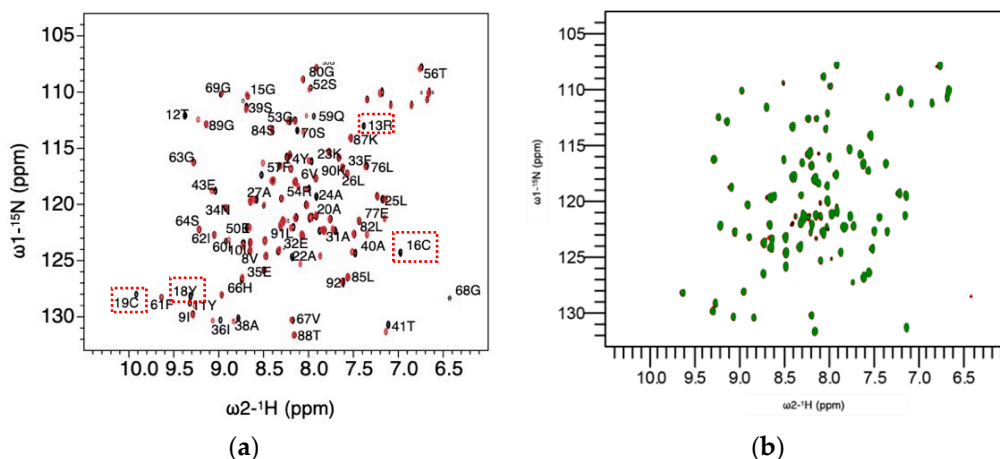


Figure 2. Chemical shift perturbation of copper ions (a) CSP of Cu(I) titrated GRX (red) reveals chemical shifts in the CPYC active site (red boxes). (b) Overlay of Cu(I) (green) and Cu(II) (red) shows nearly identical chemical shift perturbations upon ligand binding.

3.2. Cysteine Chemical Shifts Reveal Cysteine Bound to Silver

Chemical shifts of the alpha carbon ($C\alpha$) and beta carbon ($C\beta$) of cysteines are diagnostic of their chemical states, particularly their oxidation, and metal ion binding states. The values of the expected chemical shifts for cysteines participating in disulfide bonds can range from roughly 54–58 ppm for $C\alpha$ and 38–43 ppm for $C\beta$, depending on the secondary structure of the molecule [60]. Reduced thiols have $C\alpha$ and $C\beta$ chemical shifts of 56–62 ppm and 26–29 ppm, respectively (also dependent on the secondary structure). Cysteines bound to metals are known to exhibit shifts similar to those observed with reduced cysteines for $C\alpha$ and $C\beta$. Zinc binding produces chemical shifts corresponding to 59.27 ± 2.12 ppm and 30.89 ± 1.01 ppm for the $C\alpha$ and $C\beta$ respectively [61]. The previously reported NMR structure of the apo GRX from *Brucella melitensis* [62] was compared with that of the silver-metalated form (determined here), revealing differences in the cysteine's chemical shifts between the two structures (Supplemental Table S1). Both C16 and C19 have $C\beta$ shifts around 31 ppm, which is expected for the metal-liganded form of the protein. These values are consistent with other structures of proteins determined via NMR spectroscopy with CXXC metal binding motifs [54].

3.3. The NMR Structure of Silver Metalated GRX Requires Remodeling of the CPYC Active Site to Accommodate the Metal Ion

We determined the structure of a C70S mutant of the *Brucella melitensis* GRX bound to silver with a backbone RMSD of 0.6 Å (Table 2). The GRX for *Brucella melitensis* contains one cysteine (C70) that occurs outside the active site. Thus, the residue was mutated to prevent nonspecific metal interaction and/or protein aggregation during removal of chemical reductants from sample buffers. As suspected from the CSP experiments, the binding site for silver occurs in the CPYC active site. Silver metalated GRX maintains the thioredoxin like fold (Figure 3a) with a few differences from the apo structure. Structural alignment between the apo protein and the silver metalated form (Figure 3b) reveals that the structures differ on average by 1.6 Å among $C\alpha$ atoms over all residues. Helix 1 in the structure experiences significant unwinding to further open the CPYC active site that normally sits at the top of the helix. This unwinding opens up the loop region between the first β -strand and the first helix, corresponding to the residues with the largest chemical shift changes observed in the CSP experiments. Helix 2 is angled diagonally across the β -sheet in the silver-liganded structure, whereas, in the non-metalated protein this helix is generally perpendicular to the axis of the β -sheet. These large structural differences also cause other slight modifications in additional regions of the metalated protein.

Table 2. NMR Statistics.

Restraints Statistics	
Distances	1299
Short	685
Medium	258
Long	356
Dihedral	52
H-Bonds	104
Ensemble Convergence	
Backbone RMSD	0.6 ± 0.16
Heavy Atom RMSD	1.04 ± 0.14
Ramachandran Plot Statistics	
Most Favored %	79.6
Additionally Allowed %	18.9
Generously Allowed %	1.4
Disallowed %	0.0

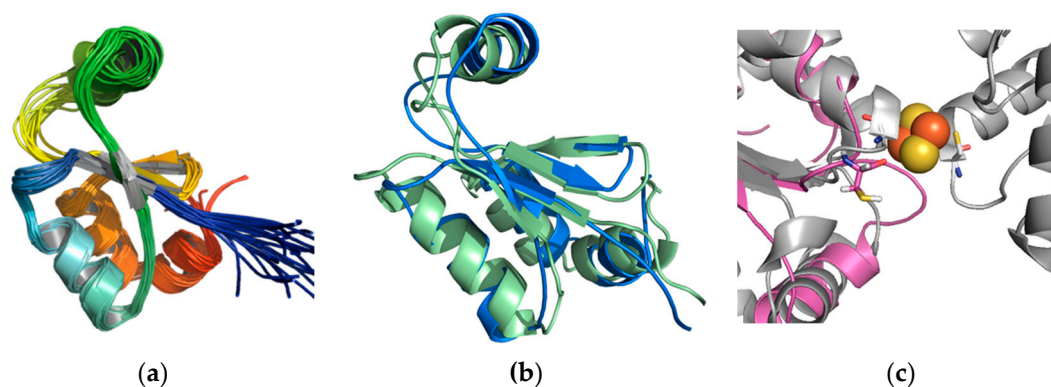


Figure 3. Structure of Ag-metalated GRX (a) ensemble structure of 20 calculated structures, (b) superposition of apo (green) and Ag-metalated protein (blue) based on an alignment of C-alphas. (c) Superposition of Ag-metalated (pink) and iron-sulfur cluster loaded structures (grey).

The silver-metalated GRX additionally contains a uniquely oriented cysteine (16C), in the CPYC active site, with the side-chain pointing outward into the solvent. This outward orientation of the first cysteine is also present in other GRXs involved in coordinating iron-sulfur clusters (Fe_2S_2) (Figure 3c) [7,8,63–65]. These GRXs coordinate an iron-sulfur cluster liganded between two cysteine side-chains, forming a dimer.

3.4. Biochemical Characterization of the Metalated Form Indicates the Protein Is a Dimer

The NMR CSP experiments indicated that a 0.5:1 (metal to protein) ratio was needed, suggesting that each monomer within a potential GRX dimer shares this metal atom. Analytical size exclusion chromatography (SEC) experiments were used to differentiate between the oligomeric states of the metalated and apo protein. SEC (Figure 4) shows that the apo, TCEP treated, and metalated (silver) protein all have nearly identical retention times, eluting at the same volume with slight differences in the elution times of high molecular weight aggregates. Based on the calibration of the column with molecular weight standards, the molecular weights of 20.95, 22.18, and 22.57 kDa correspond to the apo protein, silver metalated protein, and TCEP treated protein respectively. These values are near the expected molecular weights for the dimer (19.6 kDa). Only the excessively TCEP treated form contained later eluting shoulder that could be assigned to the monomer elution time (~10 kDa). Commonly, SEC can correlate to molecular weight, under the assumption that the protein is acting as a true sphere [66]. Based on these observations,

one can infer that the protein not only exists as a dimer at high protein concentrations, both in the presence of silver and without, but also a non-spherical shape, such as that of a prolate spheroid, contributing to the slightly faster than expected elution times for the dimer. These results are similar to SEC studies or other GRX dimers [67].

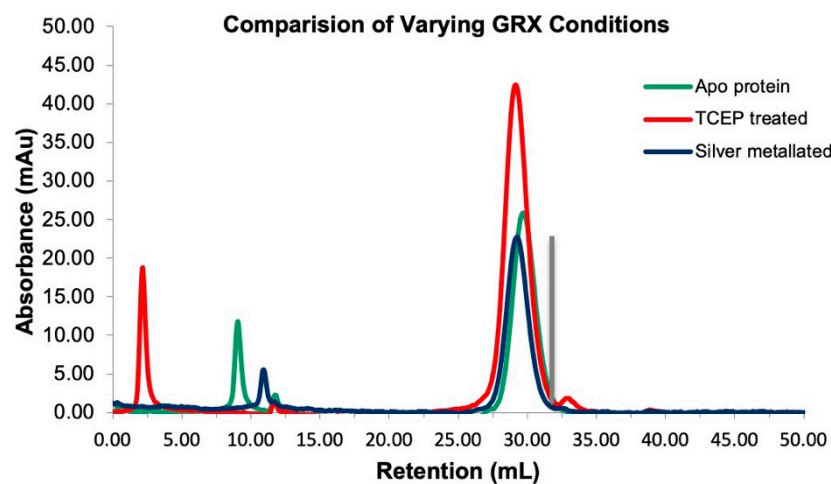


Figure 4. Size exclusion chromatography shows that the reduced apo protein (green), excess TCEP treated (red) and silver metallated protein (blue) elute at nearly identical retention volumes compatible with dimer formation.

3.5. The Silver Metallated Form of the Protein Experiences an Increase in Flexibility

The rotational correlation time (τ_c) can be used to estimate the relative molecular weight of spherical proteins [68]. Based on τ_c values previously reported, a spherical monomer of GRX with a molecular weight of 9.8 kDa should have a predicted τ_c value of 5.9 ns, with a spherical dimer τ_c value of approximately 11.92 ns. The τ_c calculated for the apo and silver metallated form of the protein were determined to be 5.89 ± 0.68 ns and 6.01 ± 0.88 ns respectively. These values are expected for a monomer in this particular experiment, contrasting the chromatography data and CSP studies. However, a closer examination of the protein dynamics reveals that several specific regions of the protein become more dynamic when metallated with silver. Residues 41T, 55N, and 56T are more flexible in the metallated form of the protein (Figure 5). Two of the residues (55N and 56T) are located in the second helix directly adjacent to the active site, inducing increased flexibility at the metal binding region of the protein. This flexibility and possible interdomain rotation and loop flexibility along with the expected prolate spheroidal shape of the dimer may reconcile the apparent discrepancy between the SEC and τ_c measurements.

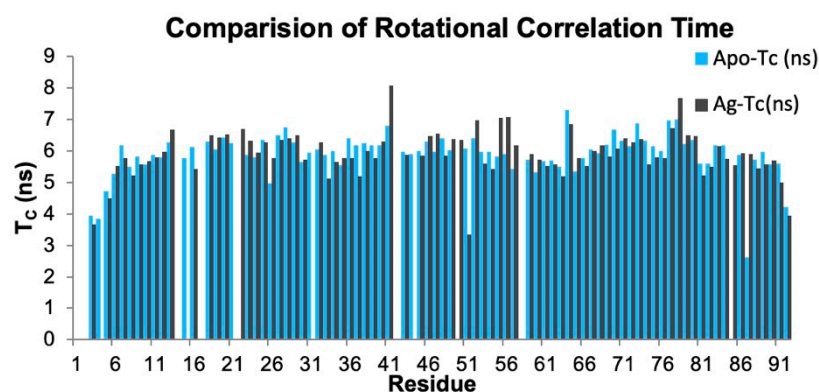


Figure 5. Rotational correlation time of both the apo and silver metallated protein. Analysis of the apo protein (blue) and the silver metallated protein (gray).

3.6. Mass-Spectrometry Reveals That the Protein Forms Metal-Mediated Dimers

GRX proteins have been implicated in forming dimers at the high concentrations used in NMR studies [69]. Our stoichiometry during NMR monitored metal titration experiments indicated that the protein was dimerized during the addition of metal ions. Electrospray ionization–mass spectrometry (ESI–MS) is a soft ionization technique that can be used to probe intact metal binding and protein dimerization, as it uses low concentrations of protein. Such low concentrations will, ideally, push the equilibrium of dimerization towards the monomer allowing for an easier observation of the effect of metal ions on the protein’s oligomeric state. The deconvoluted ESI–MS of GRX showed a monomeric mass of 10,047.5 kDa, with the addition of 0.5 equivalents of silver this mass shifted to 10,154.7 kDa (Figure 6). The difference fits the mass of one silver atom, clearly displaying metal binding. In addition to the monomeric peak, the deconvolution of the metalated GRX provides evidence of a single silver mediated dimer. One of the peaks matches a dimer mass with no silver (20,092.3), while the more intense peak matches a dimer mass with one silver bound (20,209.4). Deconvolution can be prone to creating artifacts; however, a study of the protein charge states also provides evidence of a silver mediated dimer (Supplemental Figure S2). The APO monomeric species has a charge distribution with intense peaks ranging from +10 to +4, and while the addition of silver significantly suppressed the signal intensity, the metalated monomer retains a less intense distribution of +9 to +5. The charge states +15 and +13 are also visible, which are unique to only the dimer and only are present in the metalated protein. It should be noted that the metalated monomeric peaks ranging from +11 to +5 possibly contain additional overlap of charge states +18, +16, +14, +12, and +10 from the dimer. Although electrospray conditions can result in largely unfolded species, and dimer dissociation, the addition of silver to GRX produced peaks consistent with both a silver-bound monomer and silver mediated dimer.

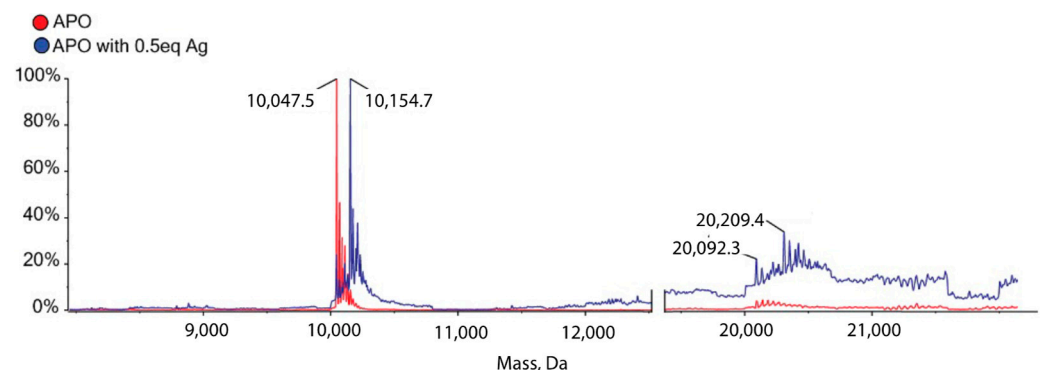


Figure 6. Deconvoluted ESI–MS of apo protein (red) and silver metalated protein (blue). Peaks labeled from left to right correspond to masses matching the monomer, the monomer with one silver, the dimer, and the dimer with one silver. The Y-axis represents relative intensity of the observed ions.

3.7. Gadolinium Reveals Dimerization Interface

Paramagnetic agents like gadolinium diethylenetriamine penta-acetic acid (Gd-DTPA) can be used to identify non-surface exposed atoms in the protein, because they do not experience any broadening effects from the paramagnetic reagent [70]. This makes Gd-DTPA an ideal tool for probing the contacts between two protein interfaces [71,72]. When the silver-metalated form of the protein was treated with Gd-DTPA, the resonances that were protected from the broadening effect clustered along the CPYC active site (Figure 7a,c). These same resonances in the apo protein were also protected from Gd-DTPA broadening effects (Figure 7b,d). These similarities between the apo and metalated protein indicate that the protein takes advantage of a natural dimerization interface and forms a dimer in both the apo and silver metalated forms of the protein at the concentrations used for NMR experiments.

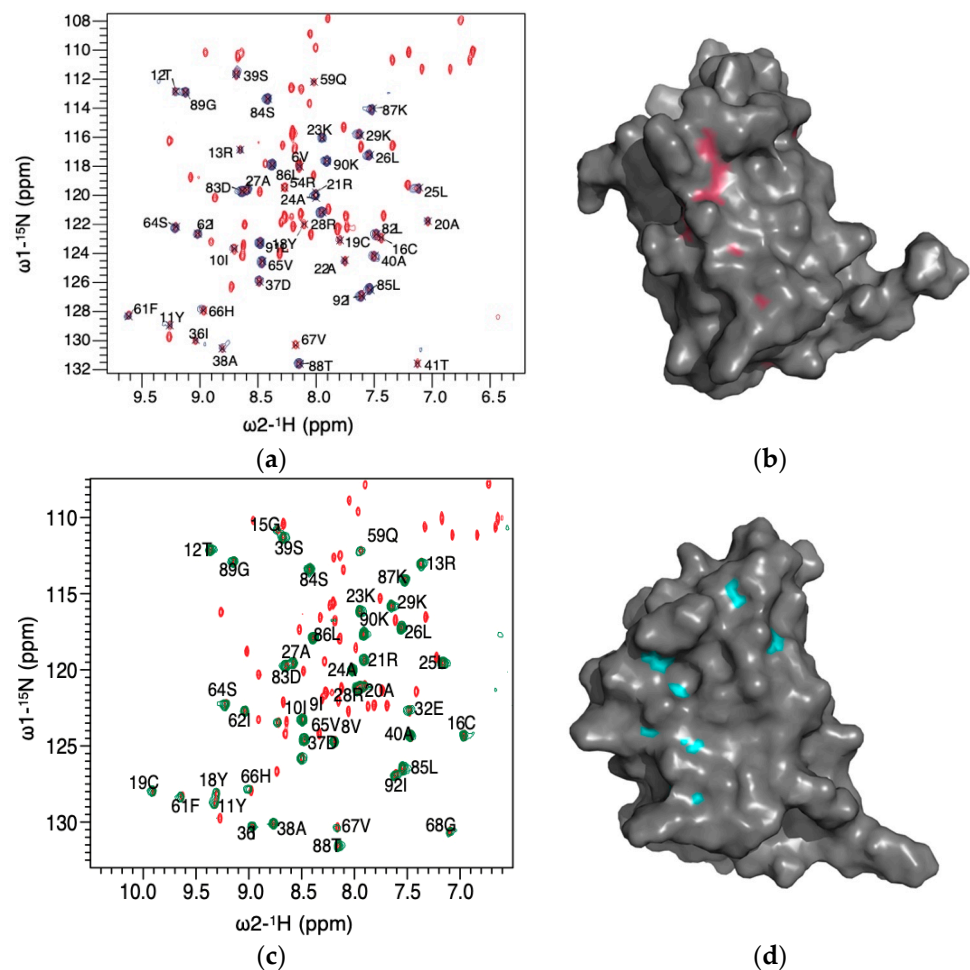


Figure 7. Gd(III) relaxation of GRX shows possible dimer interface. (a) ^{15}N -HSQC spectrum with select assignments shown 0.5 eq Ag metalated GRX (red), 0.5 eq Ag metalated GRX with 3 mM Gd-DTPA (blue); (b) solvent exposed residues protected from broadening mapped onto GRX (pink); (c) apoGRX (red) with 3 mM Gd-DTPA (green); (d) solvent exposed residues protected from broadening mapped onto the apo structure (teal) (PDB: 2KHP).

3.8. Molecular Dynamics Indicates Possible Dimer Structure

The combined set of biophysical and bioanalytical data indicates that GRX is a dimer in the presence of silver ions. The model of the dimer (Figure 8c) indicates that the metalated form of the protein is an elongated structure with the two monomers binding to the ion through the side-chain of 16C. MUSTANG alignment between the silver metalated dimer model and that of *E. coli* Fe_2S_2 GRX reveals a difference of 2.1 Å between the structures over the $\text{C}\alpha$ atoms with a 27.83% sequence homology. The major structural differences between the two proteins occur at the active site and at the second helix in the silver metalated GRX (helix 3 in the *E. coli* Fe_2S_2 GRX) (Figure 8b). At the active site in the silver metalated form of the protein, the helix is unwound and creates a larger turn prior to the helix that is not observed in the crystal structure of the *E. coli* Fe_2S_2 GRX. In the second helix (3rd helix in the Fe_2S_2 GRX), the silver metalated structure helix is rotated by 45°. This similarity between the dimeric Fe_2S_2 containing GRXs and silver metalated GRX strongly supports the data, suggesting that GRX forms a dimer around a silver atom that is branched through the first cysteine in the active site.

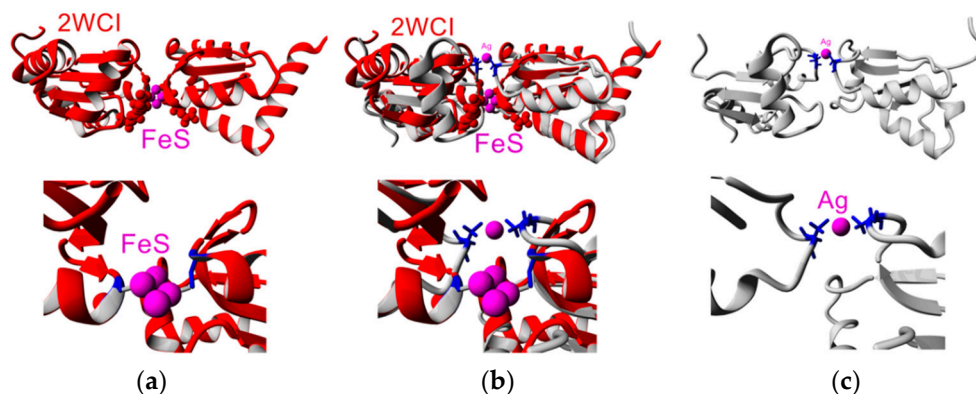


Figure 8. Comparison of global structure of dimeric GRX and their active sites. (a) The Fe-S GRX from *E. coli* (PDB: 2WCI); (b) overlay with Fe-S GRX from *E. coli* (PDB: 2WCI) (red) with silver metalated GRX (gray); (c) the model of the silver metalated dimer structure; 16C is shown in blue.

The MDs simulations also indicate differences between the monomer and dimeric form of the protein where the CPYC site is less flexible in the dimer but other regions of the protein namely along helix two are more flexible in the dimer (Figure 9). This corroborates the relaxation experiments on the apo and metalated proteins showing differences in specific amino acid flexibility between the two forms. Models of the monomer and the dimer show that the CPYC active site is less flexible in the dimer structure, which explains the decrease in τ_c at residue 16C and the increases around the residues in the second helix. This also correlates well with the predicted structure, as the metalation interface would be more rigid than that of a monomer.

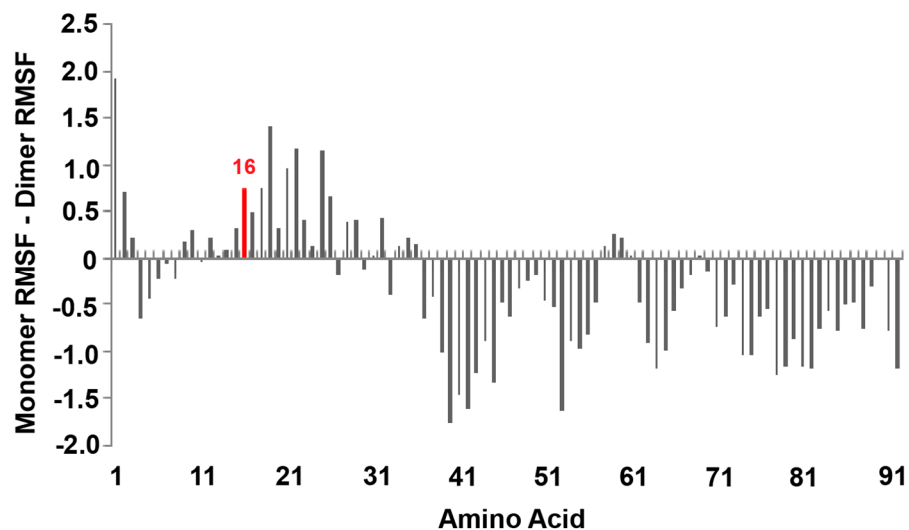


Figure 9. Amino acid movement (root mean squared fluctuation, RMSF) during MD simulations for the NMR generated model (monomer) relative to the modeled metalated dimer structure following 10 nanoseconds of MD. Data is shown as the movement of the monomer minus the dimer; amino acids with positive values have higher movement in the monomer while negative values have higher movement in the dimer.

3.9. Glutathione Cannot Completely Out-Compete Metal Ions out of the Active Site

Glutathione (GSH) is a natural ligand for GRX and binds in the CPYC active site where several metals have been presented to bind. CSP studies of the metalated form of both the copper and silver titrated protein show that GSH addition induces chemical shift changes in the spectrum (Figure 10a,b) and are indicative of fast exchange between GSH bound and unbound forms relative to the chemical shift timescale. However, these

chemical shift changes do not return the protein spectrum to that of the apo spectrum or that of the spectrum of the GSH bound protein (Supplemental Figure S3), indicating that the GSH is not removing the metal ion from the active site, or binding in its place. Therefore, while GSH does have an impact on the metalated form of the protein it is likely unable to compete with the metal ion bound in the active site for the 16C thiolate.

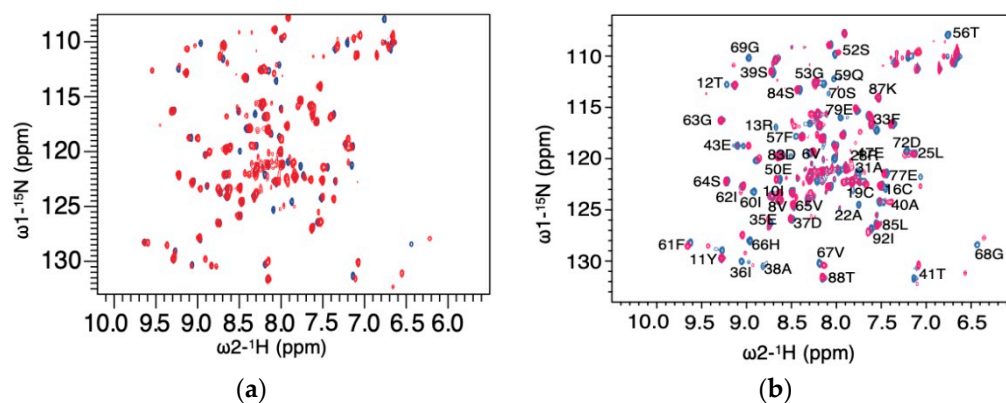


Figure 10. Competitions Studies with GSH (a) Cu(I) metalated GRX (blue) with 3.5 eq GSH (red); (b) Ag(I) titrated GRX (blue), 16 mM GSH with 0.5 eq silver titrated GRX (pink).

3.10. Enzymology Supports Silver-Mediated Dimer Inactivation

The enzymatic rate of GRX was observed using the bis(2-hydroxyethyl) disulfide (HEDS) assay, a classical experiment that measures deglutathionylation activity by monitoring oxidation of NADPH at 340 nm in a reaction that couples GRX and glutathione reductase. During a preincubation phase, GSH and HEDS spontaneously react to form a heterodisulfide. When GRX is introduced, it catalyzes deglutathionylation of the disulfide producing oxidized GSH. As quickly as it is made, oxidized GSH is in turn reduced by glutathione reductase, which consumes NADPH in a redox reaction. Activity plotted as a function of GRX concentration produces an activity trend that plateaus as the maximum concentration tested is approached (Figure 11a). While the trend line plotted through the first few apo points predicts the expected activity, curves that depict this type of activity for GRX concentrations above 1 μM have been previously described in HEDS assays [73]. The statistical reduction in activity upon the addition of silver even at the highest concentrations of GRX in our protocol confirms the HEDS assay as an acceptable system to monitor dimerization despite a concentration dependence of the activity on GRX itself that is not well understood.

Silver dependent reduction in activity at a constant GRX concentration can be easily observed from raw absorbance data (Figure 11b). The first 30 s these curves were used to calculate GRX activity as a function of mM of NADPH oxidized/min. The resulting trends with increasing silver result in sigmoidal activity curves (Figure 11c). The reciprocal values of these were used to produce Dixon plots showing an upward parabolic curve with slopes increasing along with silver concentration (Figure 11d). Dixon curves with parabolic trends have previously been described to explain enzyme inhibition with compounds interacting at multiple binding sites [74,75]. We propose that these trends also can describe inhibition in shared metal complexes: where one atom of silver can inhibit two molecules of GRX, an exponential increase in the rate of inhibition is expected. These results support our dimeric inhibition model, as it would not be possible to produce parabolic Dixon plots without an effective stoichiometric inhibition ratio greater than 1:1.

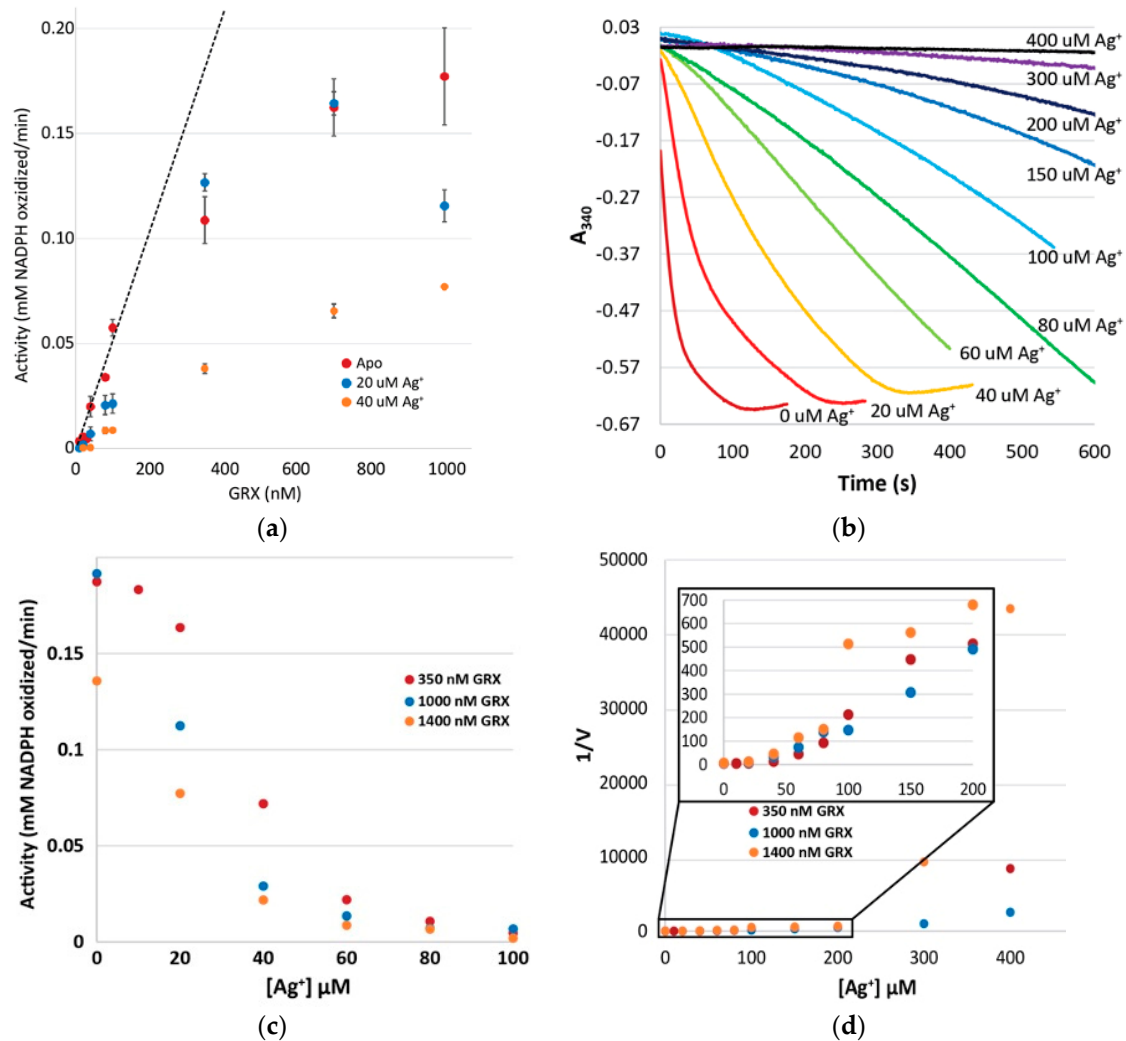


Figure 11. GRX activity under varying enzyme and silver concentrations. (a) A range of GRX concentrations were measured in triplicate as apo protein and inhibited with two constant silver concentrations. The dashed line indicates theoretical apo rate. Calculated activity as NADPH consumed over time from the HEDS assay. (b) Raw absorbance data from silver inhibition with 1400 nM GRX. Plotting activity from these data (c) produces inhibition plots that show a sigmoidal trend as a function of increasing silver. (d) Dixon plots of the reciprocal activity give rise to parabolic trends that support dimer inactivation.

4. Discussion

Several studies have tied GRX function to the maintenance of the redox environment and its essential importance to copper chaperones [10,11,15]. The CPYC site of GRX is typically used in the reduction of disulfide bonds, but shares many similarities with the CXXC motif found in metal binding domains. Therefore, it is possible that the CPYC could also bind metals. It had been initially suggested that the proline in the CPYC active site prevents metal binding due to the limiting backbone torsion flexibility; flexibility that was presumed to be required for both cysteines to coordinate a metal ion within the monomer [14]. Past assumptions that limited backbone flexibility prevents co-ligation to the metal by the CPYC thiols is not entirely relevant, since GRX uses intermolecular coordination to the metal. The proline may indeed prevent simultaneous C16–C19 coordination to the metal, but it does not prevent intermolecular associations involving residue C16. Recent biochemical experiments have shown that hGRX can bind to Cu(I) but with a lower affinity than the other proteins within the cytosol [15]. In fact, of all the iron–sulfur coordinated GRXs whose structures have been elucidated, none of these proteins contains a proline in the active site. We have presented here the first structure of a GRX with its native CPYC active

site bound to a metal ion, in this case silver(I). The binding to the CPYC active site shows that not only can silver bind to a protein, but it binds to a protein in a manner that has implications for the mechanism of action of silver ions as antimicrobials. The antimicrobial effects of silver have been attributed to many mechanisms ranging from an increase in ROS [28] to induction of morphology changes in the cell wall [76]. It is this interaction with ROS species that is of most interest in light of our results. GRX has been shown to interact with both ATP7a and ATP7b proteins [12], with ATP7b implicated in having a possible role in detoxifying silver ions in the lungs [77]. The intermolecular association of GRXs to form metal mediated dimers is provocatively similar to the proposed hand-off mechanism for ATOX1 with other proteins [78]. While there is no conclusive evidence that GRXs act as general metal cation chaperones, the structures reported here, along with the ATP7a and ATP7b association and the extensive work on iron–sulfur cluster transfer, support the notion that GRXs may transfer a variety of metals between proteins, and that disruption of those transfers by xenobiotic metals may lead to ROS accumulation. It is possible that our proposed mechanism for dimerization is unique to the GRX1 from *Brucella melitensis*. This protein was chosen for study due to its well-resolved NMR spectra; however, the NMR techniques for monitoring metal binding and the dimerization interface described herein could be applied to other GRXs.

The GSH competition studies with metalated GRXs provide further indication that metal ions could work to disrupt cell redox systems. Once metalated, GSH does not have the ability to out-compete the metal from the protein active site. This inability is a key indicator that metal binding to GRX can either deactivate the enzyme or severely disrupt its function. This downstream effect from perturbations to GRX has been observed in knockdown experiments with shRNA where silencing of GRX-1 not only increased the susceptibility of ROS but also perturbed other proteins in the antioxidant pool [79].

In addition to the structure of the silver metalated form of the protein, we have shown here via CSP studies that several different metals can bind to the active site of GRX. While past studies have shown that GRX will bind to metals such as copper [15] or mercury [9], which we have confirmed as distinctly binding in the CPYC active site. Our titration data also indicates that the protein favors a dimer in the presence of silver(I), which is further supported by enzymology, SEC chromatography, and MD simulations, and that the structure adopted is similar to other GRX dimers containing an iron–sulfur cluster [7]. Future studies are required to determine if this dimerization is biologically relevant in cells but suggests new avenues for stimulating ROS-mediated antibiotics via metal-based or small molecule warheads that deplete the active GRX pool through dimerization.

Supplementary Materials: The following are available online at <https://www.mdpi.com/article/10.3390/biophysica1040027/s1>, Figure S1: Chemical shift perturbation of Hg(II). Figure S2: Overlapped ESI-MS spectra of apo protein (red) and silver metalated protein (blue). Figure S3: CSP with GSH. GRX titrated with increasing concentrations of GSH. Table S1: Chemical shifts of the cysteine carbons in the active site.

Author Contributions: Conceptualization, S.M.B. and T.C.L.; methodology, S.M.B., D.L.M., J.W.P., J.A.C., A.T., N.D., M.J.P. and T.C.L.; writing—original draft preparation, S.M.B. and T.C.L.; writing—review and editing, S.M.B., D.L.M. and T.C.L.; supervision L.P.S. and T.C.L.; project administration, T.C.L. All authors have read and agreed to the published version of the manuscript.

Funding: The Kresge Foundation supported acquisition and upkeep of the 750 Mhz NMR spectrometer at the University of Akron where the NMR data were collected. S.M.B. received the Choose Ohio First Bioinformatics Scholarships for computer upgrades. University of Akron Buchtel College of Arts and Science Student Research Scholarships funded work performed by graduate researchers S.M.B. and undergraduate researchers N.D.

Data Availability Statement: Ensemble atomic coordinates for the GRX metal mediated dimer are available in the Protein Data Bank (PDB Entry 2mzc) and assigned chemical shifts are available in the Biological Magnetic Resonance Data Bank (BMRB Entry 25483).

Acknowledgments: We would like to acknowledge Wiley Youngs at the University of Akron for his inspiration and advice regarding silver chemistry and reactivity with proteins. Undergraduate student researchers contributed in small ways to this work and should be acknowledged: Brandon Rapier and Jacob Sweet.

Conflicts of Interest: The authors declare no conflict of interest.

References

1. Lillig, C.H.; Berndt, C.; Holmgren, A. Glutaredoxin systems. *Biochim. Biophys. Acta* **2008**, *1780*, 1304–1317. [[CrossRef](#)] [[PubMed](#)]
2. Liedgens, L.; Zimmermann, J.; Wäschenbach, L.; Geissel, F.; Laporte, H.; Gohlke, H.; Morgan, B.; Deponte, M. Quantitative assessment of the determinant structural differences between redox-active and inactive glutaredoxins. *Nat. Commun.* **2020**, *11*, 1–18. [[CrossRef](#)] [[PubMed](#)]
3. Trnka, D.; Engelke, A.D.; Gellert, M.; Moseler, A.; Hossain, M.F.; Lindenberg, T.T.; Pedroletti, L.; Odermatt, B.; de Souza, J.V.; Bronowska, A.K.; et al. Molecular basis for the distinct functions of redox-active and FeS-transferring glutaredoxins. *Nat. Commun.* **2020**, *11*, 1–12.
4. Banci, L.; Baffoni, S.C.; Gajda, K.; Muzzioli, R.; Peruzzini, R.; Winkelmann, J. N-terminal domains mediate [2Fe-2S] cluster transfer from glutaredoxin-3 to anamorsin. *Nat. Chem. Biol.* **2015**, *11*, 772–778. [[CrossRef](#)] [[PubMed](#)]
5. Shi, J.; Vlamis-Gardikas, A.; Åslund, F.; Holmgren, A.; Rosen, B.P. Reactivity of Glutaredoxins 1, 2, and 3 from *Escherichia coli* shows that Glutaredoxin 2 is the primary hydrogen donor to arsc-catalyzed arsenate reduction. *J. Biol. Chem.* **1999**, *274*, 36039–36042. [[CrossRef](#)] [[PubMed](#)]
6. Gladysheva, T.B.; Oden, K.L.; Rosen, B.P. Properties of the Arsenate Reductase of Plasmid R773. *Biochemistry* **1994**, *33*, 7288–7293. [[CrossRef](#)]
7. Johansson, C.; Kavanagh, K.L.; Gileadi, O.; Oppermann, U. Reversible sequestration of active site cysteines in a 2Fe-2S-bridged dimer provides a mechanism for Glutaredoxin 2 regulation in human mitochondria. *J. Biol. Chem.* **2007**, *282*, 3077–3082. [[CrossRef](#)]
8. Rouhier, N.; Unno, H.; Bandyopadhyay, S.; Masip, L.; Kim, S.K.; Hirasawa, M.; Gualberto, J.M.; Lattard, V.; Kusunoki, M.; Knaff, D.B.; et al. Functional, structural, and spectroscopic characterization of a glutathione-ligated [2Fe-2S] cluster in poplar glutaredoxin C1. *Proc. Natl. Acad. Sci. USA* **2007**, *104*, 7379–7384. [[CrossRef](#)]
9. Carvalho, C.; Chew, E.-H.; Hashemy, S.I.; Lu, J.; Holmgren, A. Inhibition of the human thioredoxin system. A molecular mechanism of mercury toxicity. *J. Biol. Chem.* **2008**, *283*, 11913–11923. [[CrossRef](#)]
10. Lim, C.M.; Cater, M.A.; Mercer, J.F.; La Fontaine, S. Copper-dependent interaction of glutaredoxin with the N termini of the copper-ATPases (ATP7A and ATP7B) defective in Menkes and Wilson diseases. *Biochem. Biophys. Res. Commun.* **2006**, *348*, 428–436. [[CrossRef](#)]
11. Hatori, Y.; Clasen, S.; Hasan, N.M.; Barry, A.; Lutsenko, S. Functional partnership of the copper export machinery and glutathione balance in human cells. *J. Biol. Chem.* **2012**, *287*, 26678–26687. [[CrossRef](#)] [[PubMed](#)]
12. Singleton, W.C.; McInnes, K.T.; Cater, M.A.; Winnall, W.R.; McKirdy, R.; Yu, Y.; Taylor, P.E.; Ke, B.-X.; Richardson, D.; Mercer, J.F.; et al. Role of Glutaredoxin1 and Glutathione in regulating the activity of the copper-transporting P-type ATPases, ATP7A and ATP7B. *J. Biol. Chem.* **2010**, *285*, 27111–27121. [[CrossRef](#)] [[PubMed](#)]
13. Mercer, S.W.; Burke, R. Evidence for a role for the putative *Drosophila* hGRX1 orthologue in copper homeostasis. *BioMetals* **2016**, *29*, 705–713. [[CrossRef](#)] [[PubMed](#)]
14. Su, D.; Berndt, C.; Fomenko, D.E.; Holmgren, A.; Gladyshev, V.N. A Conserved cis-proline precludes metal binding by the active site thiolates in members of the thioredoxin family of proteins. *Biochemistry* **2007**, *46*, 6903–6910. [[CrossRef](#)] [[PubMed](#)]
15. Brose, J.; La Fontaine, S.; Wedd, A.G.; Xiao, Z. Redox sulfur chemistry of the copper chaperone Atox1 is regulated by the enzyme glutaredoxin 1, the reduction potential of the glutathione couple GSSG/2GSH and the availability of Cu(i). *Metallomics* **2014**, *6*, 793–808. [[CrossRef](#)]
16. Maghool, S.; La Fontaine, S.; Roberts, B.R.; Kwan, A.H.; Maher, M.J. Human glutaredoxin-1 can transfer copper to isolated metal binding domains of the P1B-type ATPase, ATP7B. *Sci. Rep.* **2020**, *10*, 4157. [[CrossRef](#)] [[PubMed](#)]
17. Hoffmann, B.; Uzarska, M.A.; Berndt, C.; Godoy, J.R.; Haunhorst, P.; Lillig, C.H.; Lill, R.; Mühlhoff, U. The multidomain thioredoxin-monothiol glutaredoxins represent a distinct functional group. *Antioxid. Redox Signal* **2011**, *15*, 19–30. [[CrossRef](#)]
18. Manta, B.; Pavan, C.; Sturlese, M.; Medeiros, A.; Crispo, M.; Berndt, C.; Krauth-Siegel, R.L.; Bellanda, M.; Comini, M.A. Iron-sulfur cluster binding by mitochondrial monothiol glutaredoxin-1 of *Trypanosoma brucei*: Molecular basis of iron-sulfur cluster coordination and relevance for parasite infectivity. *Antioxid. Redox Signal* **2013**, *19*, 665–682. [[CrossRef](#)]
19. Roret, T.; Zhang, B.; Moseler, A.; Dhalleine, T.; Gao, X.H.; Couturier, J.; Lemaire, S.D.; Didierjean, C.; Johnson, M.K.; Rouhier, N. Atypical Iron-Sulfur Cluster Binding, Redox Activity and Structural Properties of *Chlamydomonas reinhardtii* Glutaredoxin 2. *Antioxidants* **2021**, *10*, 803. [[CrossRef](#)]
20. Ceylan, S.; Seidel, V.; Ziebart, N.; Berndt, C.; Dirdjaja, N.; Krauth-Siegel, R.L. The dithiol glutaredoxins of African trypanosomes have distinct roles and are closely linked to the unique trypanothione metabolism. *J. Biol. Chem.* **2010**, *285*, 35224–35237. [[CrossRef](#)] [[PubMed](#)]
21. Xiao, Z.; La Fontaine, S.; Bush, A.I.; Wedd, A.G. Molecular mechanisms of glutaredoxin enzymes: Versatile hubs for thiol-disulfide exchange between protein thiols and glutathione. *J. Mol. Biol.* **2018**, *431*, 158–177. [[CrossRef](#)]

22. Fox, C.L., Jr. Silver sulfadiazine—A new topical therapy for Pseudomonas in burns. Therapy of Pseudomonas infection in burns. *Arch. Surg.* **1968**, *96*, 184–188. [[CrossRef](#)]
23. Wright, B.D.; Shah, P.N.; McDonald, L.J.; Shaeffer, M.L.; Wagers, P.O.; Panzner, M.J.; Smolen, J.; Tagaev, J.; Tessier, C.A.; Cannon, C.; et al. Synthesis, characterization, and antimicrobial activity of silver carbene complexes derived from 4,5,6,7-tetrachlorobenzimidazole against antibiotic resistant bacteria. *Dalton Trans.* **2012**, *41*, 6500–6506. [[CrossRef](#)] [[PubMed](#)]
24. Kascatan-Nebioglu, A.; Melaiye, A.; Hindi, K.; Durmus, S.; Panzner, M.J.; Hogue, L.A.; Mallett, R.J.; Hovis, C.E.; Coughenour, M.; Crosby, S.D.; et al. Synthesis from caffeine of a MixedN-heterocyclic carbene—silver acetate complex active against resistant respiratory pathogens. *J. Med. Chem.* **2006**, *49*, 6811–6818. [[CrossRef](#)] [[PubMed](#)]
25. Frei, A.; Zuegg, J.; Elliott, A.G.; Baker, M.V.; Braese, S.; Brown, C.; Chen, F.; Dowson, C.G.; Dujardin, G.; Jung, N.; et al. Metal complexes as a promising source for new antibiotics. *Chem. Sci.* **2020**, *11*, 2627–2639. [[CrossRef](#)] [[PubMed](#)]
26. Sharkey, M.A.; O’Gara, J.P.; Gordon, S.V.; Hackenberg, F.; Healy, C.; Paradisi, F.; Patil, S.; Schaible, B.; Tacke, M. Investigations into the antibacterial activity of the silver-based antibiotic drug candidate SBC. *Antibiotics* **2012**, *1*, 25–28. [[CrossRef](#)]
27. Palomero, O.E.; Cunningham, A.L.; Davies, B.W.; Jones, R.A. Antibacterial thiamine inspired silver (I) and gold (I) N-heterocyclic carbene compounds. *Inorg. Chim. Acta* **2020**, *517*, 120152. [[CrossRef](#)] [[PubMed](#)]
28. Siciliano, T.J.; Deblock, M.C.; Hindi, K.M.; Durmus, S.; Panzner, M.J.; Tessier, C.A.; Youngs, W.J. Synthesis and anticancer properties of gold(I) and silver(I) N-heterocyclic carbene complexes. *J. Organomet. Chem.* **2011**, *696*, 1066–1071. [[CrossRef](#)]
29. Holmes, J.; Kearsey, R.J.; Paske, K.A.; Singer, F.N.; Atallah, S.; Pask, C.M.; Phillips, R.M.; Willans, C.E. Tethered N-heterocyclic carbene-carboranyl silver complexes for cancer therapy. *Organometallics* **2019**, *38*, 2530–2538. [[CrossRef](#)]
30. Ceramella, J.; Mariconda, A.; Iacopetta, D.; Saturnino, C.; Barbarossa, A.; Caruso, A.; Rosano, C.; Sinicropi, M.S.; Longo, P. From coins to cancer therapy: Gold, silver and copper complexes targeting human topoisomerases. *Bioorganic Med. Chem. Lett.* **2020**, *30*, 126905. [[CrossRef](#)]
31. Kankala, S.; Thota, N.; Björkling, F.; Taylor, M.K.; Vadde, R.; Balusu, R. Silver carbene complexes: An emerging class of anti-cancer agents. *Drug Dev. Res.* **2019**, *80*, 188–199. [[CrossRef](#)] [[PubMed](#)]
32. Morones-Ramirez, J.R.; Winkler, J.A.; Spina, C.; Collins, J.J. Silver enhances antibiotic activity against gram-negative bacteria. *Sci. Transl. Med.* **2013**, *5*, 190ra81. [[CrossRef](#)] [[PubMed](#)]
33. Park, H.-J.; Kim, J.Y.; Kim, J.; Lee, J.-H.; Hahn, J.-S.; Gu, M.B.; Yoon, J. Silver-ion-mediated reactive oxygen species generation affecting bactericidal activity. *Water Res.* **2009**, *43*, 1027–1032. [[CrossRef](#)]
34. Gordon, O.; Slenters, T.V.; Brunetto, P.S.; Villaruz, A.E.; Sturdevant, D.E.; Otto, M.; Landmann, R.; Fromm, K.M. Silver coordination polymers for prevention of implant infection: Thiol interaction, impact on respiratory chain enzymes, and hydroxyl radical induction. *Antimicrob. Agents Chemother.* **2010**, *54*, 4208–4218. [[CrossRef](#)] [[PubMed](#)]
35. Das, B.; Dash, S.K.; Mandal, D.; Ghosh, T.; Chattopadhyay, S.; Tripathy, S.; Das, S.; Dey, S.K.; Das, D.; Roy, S. Green synthesized silver nanoparticles destroy multidrug resistant bacteria via reactive oxygen species mediated membrane damage. *Arab. J. Chem.* **2017**, *10*, 862–876. [[CrossRef](#)]
36. Liao, S.Y.; Read, D.C.; Pugh, W.J.; Furr, J.R.; Russell, A.D. Interaction of silver nitrate with readily identifiable groups: Relationship to the antibacterial action of silver ions. *Lett. Appl. Microbiol.* **1997**, *25*, 279–283. [[CrossRef](#)]
37. Nagy, A.; Harrison, A.; Sabbani, S.; Munson, R.S., Jr.; Dutta, P.K.; Waldman, W.J. Silver nanoparticles embedded in zeolite membranes: Release of silver ions and mechanism of antibacterial action. *Int. J. Nanomed.* **2011**, *6*, 1833–1852.
38. Sattler, M.; Schleucher, J.; Griesinger, C. Heteronuclear multidimensional NMR experiments for the structure determination of proteins in solution employing pulsed field gradients. *Prog. Nucl. Magn. Reson. Spectrosc.* **1999**, *34*, 93–158. [[CrossRef](#)]
39. Delaglio, F.; Grzesiek, S.; Vuister, G.; Zhu, G.; Pfeifer, J.; Bax, A. NMRPipe: A multidimensional spectral processing system based on UNIX pipes. *J. Biomol. NMR* **1995**, *6*, 277–293. [[CrossRef](#)]
40. Vranken, W.; Boucher, W.; Stevens, T.J.; Fogh, R.H.; Pajon, A.; Llinas, M.; Ulrich, E.L.; Markley, J.L.; Ionides, J.; Laue, E.D. The CCPN data model for NMR spectroscopy: Development of a software pipeline. *Proteins Struct. Funct. Bioinform.* **2005**, *59*, 687–696. [[CrossRef](#)]
41. Cheung, M.-S.; Maguire, M.L.; Stevens, T.J.; Broadhurst, R.W. DANGLE: A Bayesian inferential method for predicting protein backbone dihedral angles and secondary structure. *J. Magn. Reson.* **2010**, *202*, 223–233. [[CrossRef](#)] [[PubMed](#)]
42. Güntert, P.; Mumenthaler, C.; Wüthrich, K. Torsion angle dynamics for NMR structure calculation with the new program Dyana. *J. Mol. Biol.* **1997**, *273*, 283–298. [[CrossRef](#)] [[PubMed](#)]
43. Güntert, P. Automated NMR structure calculation with CYANA. In *Protein NMR Techniques*; Humana Press: Totowa, NJ, USA, 2004; pp. 353–378.
44. Berman, H.M.; Westbrook, J.; Feng, Z.; Gilliland, G.; Bhat, T.N.; Weissig, H.; Shindyalov, I.M.; Bourne, P.E. The protein data bank. *Nucleic Acids Res.* **2000**, *28*, 235–242. [[CrossRef](#)]
45. Konagurthu, A.; Whistock, J.; Stuckey, P.; Lesk, A. MUSTANG: A multiple structural alignment algorithm. *Proteins Struct. Funct. Bioinform.* **2006**, *64*, 559–574. [[CrossRef](#)]
46. Morris, G.; Huey, R.; Lindstrom, W.; Sanner, M.F.; Belew, R.K.; Goodsell, D.S.; Olson, A.J. AutoDock4 and AutoDockTools4: Automated docking with selective receptor flexibility. *J. Comput. Chem.* **2009**, *30*, 2785–2791. [[CrossRef](#)]
47. Duan, Y.; Wu, C.; Chowdhury, S.; Lee, M.C.; Xiong, G.; Zhang, W.; Yang, R.; Cieplak, P.; Luo, R.; Lee, T.; et al. A point-charge force field for molecular mechanics simulations of proteins based on condensed-phase quantum mechanical calculations. *J. Comput. Chem.* **2003**, *24*, 1999–2012. [[CrossRef](#)]

48. Nagai, S.; Black, S. A Thiol-disulfide transhydrogenase from yeast. *J. Biol. Chem.* **1968**, *243*, 1942–1947. [[CrossRef](#)]
49. Zaffagnini, M.; Michelet, L.; Massot, V.; Trost, P.; Lemaire, S. Biochemical characterization of glutaredoxins from *Chlamydomonas reinhardtii* reveals the unique properties of a chloroplastic CGFS-type glutaredoxin. *J. Biol. Chem.* **2008**, *283*, 8868–8876. [[CrossRef](#)]
50. Gitschier, J.; Moffat, B.; Reilly, D.; Wood, W.I.; Fairbrother, W.J. Solution structure of the fourth metal-binding domain from the Menkes copper-transporting ATPase. *Nat. Genet.* **1998**, *5*, 47–54. [[CrossRef](#)]
51. Changela, A.; Chen, K.; Xue, Y.; Holschen, J.; Outten, C.E.; O'Halloran, T.V.; Mondragón, A. Molecular basis of metal-ion selectivity and zeptomolar sensitivity by CueR. *Science* **2003**, *301*, 1383–1387. [[CrossRef](#)]
52. Xue, Y.; Davis, A.V.; Balakrishnan, G.; Stasser, J.P.; Staehlin, B.M.; Focia, P.; Spiro, T.G.; Penner-Hahn, J.E.; O'Halloran, T.V. Cu(I) recognition via cation- π and methio-nine interactions in CusF. *Nat. Chem. Biol.* **2008**, *4*, 107–109. [[CrossRef](#)] [[PubMed](#)]
53. Long, F.; Su, C.-C.; Zimmermann, M.; Boyken, S.; Rajashankar, K.R.; Jernigan, R.L.; Yu, E.W. Crystal structures of the CusA efflux pump suggest methionine-mediated metal transport. *Nature* **2010**, *467*, 484–488. [[CrossRef](#)]
54. Panzner, M.J.; Bilinovich, S.M.; Parker, J.A.; Bladholm, E.L.; Ziegler, C.J.; Berry, S.M.; Leeper, T.C. Isomorphous deactivation of a *Pseudomonas aeruginosa* oxidoreductase: The crystal structure of Ag(I) metallated azurin at 1.7 Å. *J. Inorg. Biochem.* **2013**, *128*, 11–16. [[CrossRef](#)] [[PubMed](#)]
55. Loftin, I.R.; Franke, S.; Blackburn, N.J.; McEvoy, M.M. Unusual Cu(I)/Ag(I) coordination of *Escherichia coli* CusF as revealed by atomic resolution crystallography and X-ray absorption spectroscopy. *Protein Sci.* **2007**, *16*, 2287–2293. [[CrossRef](#)]
56. Su, C.-C.; Yang, F.; Long, F.; Reyon, D.; Routh, M.D.; Kuo, D.W.; Mokhtari, A.K.; Van Ornam, J.D.; Rabe, K.L.; Hoy, J.A.; et al. Crystal structure of the membrane fusion protein CusB from *Escherichia coli*. *J. Mol. Biol.* **2009**, *393*, 342–355. [[CrossRef](#)] [[PubMed](#)]
57. Singh, S.K.; Roberts, S.A.; McDevitt, S.F.; Weichsel, A.; Wildner, G.F.; Grass, G.B.; Rensing, C.; Montfort, W.R. Crystal structures of multicopper oxidase CueO Bound to Copper(I) and Silver(I): Functional role of a methionine-rich sequence. *J. Biol. Chem.* **2011**, *286*, 37849–37857. [[CrossRef](#)]
58. Anastassopoulou, I.; Banci, L.; Bertini, I.; Cantini, F.; Katsari, E.; Rosato, A. Solution structure of the Apo and Copper(I)-loaded human metallochaperone HAH1. *Biochemistry* **2004**, *43*, 13046–13053. [[CrossRef](#)]
59. Brouwer, M.; Brouwer-Hoexum, T. Interaction of copper-metallothionein from the American lobster, *Homarus americanus*, with glutathione. *Arch. Biochem. Biophys.* **1991**, *290*, 207–213. [[CrossRef](#)]
60. Sharma, D.; Rajarathnam, K. ¹³C NMR chemical shifts can predict disulfide bond formation. *J. Biomol. NMR* **2000**, *18*, 165–171. [[CrossRef](#)]
61. Kornhaber, G.J.; Snyder, D.; Moseley, H.N.B.; Montelione, G.T. Identification of zinc-ligated cysteine residues based on ¹³C α and ¹³C β chemical shift data. *J. Biomol. NMR.* **2006**, *34*, 259–269. [[CrossRef](#)]
62. Leeper, T.; Zhang, S.; Van Voorhis, W.C.; Myler, P.J.; Varani, G. Comparative analysis of glutaredoxin domains from bacterial opportunistic pathogens. *Acta Crystallogr. Sect. F Struct. Biol. Cryst. Commun.* **2011**, *67*, 1141–1147. [[CrossRef](#)] [[PubMed](#)]
63. Iwema, T.; Picciocchi, A.; Traore, D.; Ferrer, J.-L.; Chauvat, F.; Jacquamet, L. Structural basis for delivery of the intact [Fe₂S₂] cluster by monothiol glutaredoxin. *Biochemistry* **2009**, *48*, 6041–6043. [[CrossRef](#)] [[PubMed](#)]
64. Johansson, C.; Roos, A.K.; Montano, S.J.; Sengupta, R.; Filippakopoulos, P.; Guo, K.; Von Delft, F.; Holmgren, A.; Oppermann, U.; Kavanagh, K.L. The crystal structure of human GLRX5: Iron–sulfur cluster co-ordination, tetrameric assembly and monomer activity. *Biochem. J.* **2011**, *433*, 303–311. [[CrossRef](#)] [[PubMed](#)]
65. Couturier, J.; Ströher, E.; Albetel, A.-N.; Roret, T.; Muthuramalingam, M.; Tarrago, L.; Seidel, T.; Tsan, P.; Jacquot, J.P.; Johnson, M.K.; et al. Arabidopsis chloroplastic glutaredoxin C5 as a model to explore molecular determinants for iron-sulfur cluster binding into glutaredoxins. *J. Biol. Chem.* **2011**, *286*, 27515–27527. [[CrossRef](#)] [[PubMed](#)]
66. Erickson, H.P. Size and shape of protein molecules at the nanometer level determined by sedimentation, gel filtration, and electron microscopy. *Biol. Proced. Online* **2009**, *11*, 32–51. [[CrossRef](#)]
67. Banci, L.; Brancaccio, D.; Baffoni, S.C.; Del Conte, R.; Gadepalli, R.; Mikolajczyk, M.; Neri, S.; Piccioli, M.; Winkelmann, J. [2Fe-2S] cluster transfer in iron-sulfur protein biogenesis. *Proc. Natl. Acad. Sci. USA* **2014**, *111*, 6203–6208. [[CrossRef](#)]
68. Rossi, P.; Swapna, G.V.T.; Huang, Y.J.; Aramini, J.M.; Anklin, C.; Conover, K.; Hamilton, K.; Xiao, R.; Acton, T.B.; Ertekin, A.; et al. A microscale protein NMR sample screening pipeline. *J. Biomol. NMR* **2009**, *46*, 11–22. [[CrossRef](#)]
69. Noguera, V.; Walker, O.; Rouhier, N.; Jacquot, J.-P.; Krimm, I.; Lancelin, J.-M. NMR reveals a novel glutaredoxin–glutaredoxin interaction interface. *J. Mol. Biol.* **2005**, *353*, 629–641. [[CrossRef](#)]
70. Petros, A.M.; Mueller, L.; Kopple, K.D. NMR identification of protein surfaces using paramagnetic probes. *Biochemistry* **1990**, *29*, 10041–10048. [[CrossRef](#)]
71. Liepinsh, E.; Baryshev, M.; Sharipo, A.; Ingelman-Sundberg, M.; Otting, G.; Mkrtchian, S. Thioredoxin fold as homodimerization module in the putative chaperone ERp29: NMR structures of the domains and experimental model of the 51 kDa dimer. *Structure* **2001**, *9*, 457–471. [[CrossRef](#)]
72. Almeida, R.M.; Geraldine, C.F.G.C.; Pauleta, S.R.; Moura, J.J.G. Gd(III) Chelates as NMR probes of protein–protein interactions. Case study: Rubredoxin and Cytochrome c₃. *Inorg. Chem.* **2011**, *50*, 10600–10607. [[CrossRef](#)] [[PubMed](#)]
73. Vlamis, A.; Åslund, F.; Spyrou, G.; Bergman, T.; Holmgren, A. Cloning, overexpression, and characterization of glutaredoxin 2, an atypical glutaredoxin from *Escherichia coli*. *J. Biol. Chem.* **1997**, *272*, 11236–11243. [[CrossRef](#)] [[PubMed](#)]
74. Mu, H.; Zhou, S.-M.; Xia, Y.; Zou, H.; Meng, F.; Yan, Y.-B. Inactivation and unfolding of the hyperthermophilic inorganic pyrophosphatase from *Thermus thermophilus* by sodium dodecyl sulfate. *Int. J. Mol. Sci.* **2009**, *10*, 2849–2859. [[CrossRef](#)] [[PubMed](#)]

-
75. Lorey, S.; Stöckel-Maschek, A.; Faust, J.; Brandt, W.; Stiebitz, B.; Gorrell, M.D.; Kähne, T.; Mrestani-Klaus, C.; Wrenger, S.; Reinhold, D.; et al. Different modes of dipeptidyl peptidase IV (CD26) inhibition by oligopeptides derived from the N-terminus of HIV-1 Tat indicate at least two inhibitor binding sites. *JBIC J. Biol. Inorg. Chem.* **2003**, *270*, 2147–2156. [[CrossRef](#)]
 76. Sondi, I.; Salopek-Sondi, B. Silver nanoparticles as antimicrobial agent: A case study on *E. coli* as a model for Gram-negative bacteria. *J. Colloid Interface Sci.* **2004**, *275*, 177–182. [[CrossRef](#)]
 77. Ibricevic, A.; Brody, S.L.; Youngs, W.J.; Cannon, C. ATP7B detoxifies silver in ciliated airway epithelial cells. *Toxicol. Appl. Pharmacol.* **2010**, *243*, 315–322. [[CrossRef](#)]
 78. Wernimont, A.K.; Huffman, D.L.; Lamb, A.; O'Halloran, T.V.; Rosenzweig, A.C. Structural basis for copper transfer by the metallochaperone for the Menkes/Wilson disease proteins. *Nat. Struct. Mol. Biol.* **2000**, *7*, 766–771.
 79. Kippner, L.E.; Finn, N.A.; Shukla, S.; Kemp, M.L. Systemic remodeling of the redox regulatory network due to RNAi perturbations of glutaredoxin 1, thioredoxin 1, and glucose-6-phosphate dehydrogenase. *BMC Syst. Biol.* **2011**, *5*, 164. [[CrossRef](#)]